MCB
Journals.ASM.org

Human Muscle LIM Protein Dimerizes along the Actin Cytoskeleton and Cross-Links Actin Filaments

Céline Hoffmann,[a] Flora Moreau,[a] Michèle Moes,[a] Carole Luthold,[a] Monika Dieterle,[a] Emeline Goretti,[b] Katrin Neumann,[a] André Steinmetz,[a] Clément Thomas[a]

Laboratory of Cellular and Molecular Oncology[a] and Laboratory of Cardiovascular Research,[b] Public Research Center for Health, Luxembourg, Luxembourg

The muscle LIM protein (MLP) is a nucleocytoplasmic shuttling protein playing important roles in the regulation of myocyte remodeling and adaptation to hypertrophic stimuli. Missense mutations in human MLP or its ablation in transgenic mice promotes cardiomyopathy and heart failure. The exact function(s) of MLP in the cytoplasmic compartment and the underlying molecular mechanisms remain largely unknown. Here, we provide evidence that MLP autonomously binds to, stabilizes, and bundles actin filaments (AFs) independently of calcium and pH. Using total internal reflection fluorescence microscopy, we have shown how MLP cross-links actin filaments into both unipolar and mixed-polarity bundles. Quantitative analysis of the actin cytoskeleton configuration confirmed that MLP substantially promotes actin bundling in live myoblasts. In addition, bimolecular fluorescence complementation (BiFC) assays revealed MLP self-association. Remarkably, BiFC complexes mostly localize along actin filament-rich structures, such as stress fibers and sarcomeres, supporting a functional link between MLP self-association and actin cross-linking. Finally, we have demonstrated that MLP self-associates through its N-terminal LIM domain, whereas it binds to AFs through its C-terminal LIM domain. Together our data support that MLP contributes to the maintenance of cardiomyocyte cytoarchitecture by a mechanism involving its self-association and actin filament cross-linking.

The three vertebrate cysteine-rich proteins (CRP1, CRP2, and CRP3, the last also known as MLP, for muscle LIM protein) define a subset of LIM domain-containing proteins which have been associated with a wide range of cellular processes, including differentiation, growth, contractility, apoptosis, and motility (1–9). CRPs typically exhibit dual nuclear and cytoplasmic localization. In the nucleus, CRPs coregulate gene expression by interacting with transcription factors involved in myogenic differentiation (1–3, 10). In the cytoplasm, they localize to actin filament (AF)-enriched structures and interact with cytoskeletal proteins (11–15). Finally, a diffuse cytosolic fraction of CRPs has repeatedly been reported. Such a diversity of localization patterns considerably complicates the elucidation of the exact function(s) of CRPs and of the underlying molecular mechanisms.

The skeletal and cardiac muscle-enriched MLP (1) has received particular attention because several point mutations are associated with dilated or hypertrophic cardiomyopathy (16–21). In addition, abnormal levels of MLP are observed in cardiomyocytes from patients with heart failure (22, 23). In support of a direct involvement of MLP in disease, both the ablation (knockout) of the *MLP* gene and the introduction (knock-in) of a point mutation relevant for human disease in mouse are sufficient to cause a severe cardiomyopathy and heart failure phenotype, as well as (milder) skeletal muscle pathology (24, 25). However, it remains unclear how MLP defects lead to or increase the risk of muscle disease.

MLP has been suggested to be part of a mechanical stress-sensing and -signaling machinery (26). In support of that view, MLP localizes to subcellular structures with pivotal roles in mechanosensation and -transduction, such as the sarcomeric Z line and the costamere (12, 18, 24, 25, 27). In addition, biomechanical stress has been shown to induce MLP translocation into the nucleus (22, 28, 29), where it promotes myogenic differentiation (1). Using biochemical subcellular fractionation, Boateng and coworkers (22) provided evidence that both monomeric and oligomeric forms of MLP are present in neonatal rat myocytes. Interestingly, the nuclear fraction exclusively contained MLP monomers, whereas the membrane and cytoskeleton fractions contained MLP di- and oligomers. Although their biological significance remains unclear, MLP di/oligomers are likely relevant to pathogenesis, as indicated by their substantial reduction in failing human hearts.

In the cytoplasm, CRPs were initially suggested to function as a scaffold protein that interacts with AFs only indirectly through the intermediate of its cytoskeletal partners (11, 13–15). However, evidence has been provided that the two other CRP family members, namely, CRP1 and CRP2, can bind to AFs in a direct manner (30–32). In addition, CRP1 was shown to promote actin bundle formation in both *in vitro* biochemical assays and live cell experiments (32, 33). Ma and coworkers (34) recently established that CRP1 functions in filopodium formation and dendritic growth in neurons. Remarkably, a truncated version of CRP1 containing the actin-bundling domain was sufficient to increase the number of filopodia and neuritic branches as efficiently as the full-length protein, supporting that the bundling activity of CRP1 is biologically relevant. Another recent study by Clark and Kadrmas (35) has concluded that the *Drosophila melanogaster* Mlp84B protein, a LIM protein highly related to vertebrate MLP, likely contributes to

Received 13 May 2014 **Accepted** 2 June 2014
Published ahead of print 16 June 2014
Address correspondence to Clément Thomas, clement.thomas@crp-sante.lu.
C.H. and F.M. contributed equally to this work.
Supplemental material for this article may be found at http://dx.doi.org/10.1128/MCB.00651-14.
Copyright © 2014, American Society for Microbiology. All Rights Reserved.
doi:10.1128/MCB.00651-14

muscle integrity through direct stabilization of AFs at their sites of anchorage.

Here, we addressed the question of whether and how human MLP directly regulates actin cytoskeleton organization and dynamics. Using a series of *in vitro* biochemical assays and live cell approaches, we have shown that MLP functions as a direct actin-binding protein that stabilizes and cross-links AFs into bundles. The increase in actin bundling induced by MLP expression in C2C12 myoblasts was evaluated by a quantitative method initially applied to plant cells (36). The formation of MLP-induced actin bundles was followed in real time by total internal reflection fluorescence (TIRF) microscopy (TIRFM), allowing bundle polarity characterization. Since several cross-linkers require dimerization to achieve the bivalent conformation necessary to cross-link AFs, MLP self-association was examined in intact living cells. BiFC analyses revealed that in the cytoplasm, MLP mainly self-associates along F-actin-rich structures, such as stress fibers and Z disks of myofibrils. Using a deletion mutant approach, we established that the N-terminal LIM domain of MLP is required for protein self-association but is dispensable for binding to AFs. In contrast, the C-terminal LIM domain is crucial for the direct interaction between MLP and actin filaments. In light of these and previously published data, we propose that MLP contributes to the cross-linking and anchoring of AFs at specific regions in the myocyte and that a dysfunction in the direct actin regulatory activities of MLP might be at the origin of heart disease.

MATERIALS AND METHODS

Plasmids and cloning. The list of PCR primers, restriction enzymes, and vectors used in this study are listed in Table S1 in the supplemental material. The vectors used for the expression of *Arabidopsis* PLIM2c in bacteria and YFP-ABD2 in plant cells were described in our previous articles (37, 38).

Cell culture and transfection. Mouse myogenic C2C12 cells were cultured and maintained in Dulbecco's modified Eagle's medium (DMEM) supplemented with 10% fetal bovine serum (FBS), penicillin (100 U/ml), and streptomycin (0.1 mg/ml) at 37°C in a humidified atmosphere containing 5% CO_2. Mouse cardiac muscle HL-1 cells were cultured on a fibronectin-gelatin substrate in Claycomb medium (39) (Sigma) supplemented with 10% FBS, norepinephrine (0.1 mM), L-glutamine (2 mM), penicillin (100 U/ml), and streptomycin (0.1 mg/ml). Cells were plated on coverslips and transfected in 6-well plates with 2 μg DNA diluted in 500 μl of Opti-MEM (or Claycomb medium for HL-1 cells) containing 5 μl (8 μl for HL-1 cells) of Lipofectamine 2000 (Invitrogen) according to the manufacturer's instructions. Forty hours after transfection, cells were transferred to Leibowitz medium for live cell imaging or fixed for staining. Cell suspensions of *Nicotiana tabacum* L. cv. Bright Yellow-2 (BY2) were cultured in the dark at 27°C on a rotary shaker (130 rpm) and subcultured weekly by 1:10 dilution. Biolistic transformation of BY2 cells with 5 μg plasmid encoding MLP fused at the C terminus or N terminus to GFP (MLP-GFP or GFP-MLP, respectively) or yellow fluorescent protein-tagged fABD2 (YFP-fABD2) was performed as described in our previous article (38). Fourteen hours after transformation, BY2 cells were labeled with rhodamine phalloidin in PME buffer [50 mM piperazine-*N*,*N*′-bis(2-ethanesulfonic acid) (PIPES) (pH 6.9), 20 mM $MgCl_2$, 50 mM EGTA, 5% dimethyl sulfoxide (DMSO), and 0.03% NP-40] and subjected to confocal microscopy.

Expression and purification of recombinant proteins. Recombinant glutathione *S*-transferase (GST)-fused MLP and MLP variants, including MLPΔLIM1, MLPΔLIM2, LIM1, and LIM2 (see Fig. S3 in the supplemental material), were expressed in *Escherichia coli* Rosetta2 (EMD Millipore) and purified using glutathione-agarose resin (Pierce) according to the manufacturer's instructions. Using thrombin (GE Healthcare), GST was cleaved off, while recombinant proteins were still bound to the resin. Recombinant 6-His-tagged CFL2 and PLIM2c were expressed in *E. coli* M15(pREP4) and purified under denaturing conditions using nickel-nitrilotriacetic acid (Ni-NTA) resin (Qiagen) according to manufacturer's instructions. Human fascin was kindly provided D. R. Kovar (40), and CFL1 was purchased from Cytoskeleton. Recombinant proteins were buffer exchanged using 10,000-molecular-weight-cutoff (MWCO) dialysis cassettes (Pierce) against 10 mM Tris (pH 6.9), 50 mM NaCl, and 1 mM dithiothreitol (DTT). For MLP and PLIM2c, dialysis buffer was supplemented with 50 μM $ZnCl_2$ and with 50 μM $ZnCl_2$ and 2 M urea, respectively. Prior to any experiment, proteins were preclarified at 100,000 × *g* during 30 min at 4°C and checked for correct molecular weight by SDS-PAGE, and their concentrations were determined by Bradford assay (Bio-Rad) using bovine serum albumin (BSA) as a standard.

Actin high- and low-speed cosedimentation assays. A 4 μM concentration of rabbit muscle actin (>99% pure; Cytoskeleton) was copolymerized with various amounts of recombinant MLP, MLP variants, or PLIM2c (the concentrations are given in the figures) for 1 h at 25°C in 5 mM Tris-HCl (pH 7.0), 0.2 mM $CaCl_2$, 50 mM KCl, 2 mM $MgCl_2$, 0.5 mM DTT, and 0.2 mM ATP. After polymerization, samples were centrifuged either at 100,000 × *g* in an Optima TLX ultracentrifuge (Beckman) for high-speed cosedimentation or at 12,000 × *g* for low-speed cosedimentation during 30 min at 4°C. The resulting pellets and supernatants were analyzed by SDS-PAGE and Coomassie brilliant blue R staining (Sigma-Aldrich). The respective amounts of MLP (high-speed cosedimentation) or actin (low-speed cosedimentation) were quantified by densitometry using the ImageJ software program (National Institutes of Health). The dissociation constant (K_d) and MLP-to-actin ratio at saturation were calculated using data from three independent high-speed cosedimentation experiments by fitting the data of bound MLP versus free MLP to a hyperbolic function using the SigmaPlot v10 software program (Systat Software). Low-speed cosedimentation assays were conducted both under the above-described standard conditions and with additional combinations of free [Ca^{2+}] (0.01 μM and 300 μM) and pH (6.2, 6.8, and 7.4) conditions. Free [Ca^{2+}] and pH were adjusted to the desired value using morpholineethanesulfonic acid (MES), PIPES, Tris, EGTA, and/or $CaCl_2$ according to Table S2 in the supplemental material. The results from three independent experiments were expressed as percentages of pelleted actin. To determine the nature of the higher-order AF structures induced by MLP, a sample aliquot was stained with Alexa Fluor 488 phalloidin (4 μM; Invitrogen) and subjected to fluorescence microscopy.

Actin polymerization and depolymerization assays. Following 30 min of preclarification at 100,000 × *g*, pyrene-labeled actin monomers (2.5 μM, 10% pyrene labeled; Cytoskeleton) in G buffer (2 mM Tris, pH 8.0, 0.2 mM $CaCl_2$, 0.4 mM DTT, and 0.2 mM ATP) were induced to polymerize by addition of a 1/10th volume of 10× F buffer (500 mM KCl, 20 mM $MgCl_2$, and 10 mM ATP) in the absence or in the presence of MLP (1.25 to 5 μM). The increase in pyrene fluorescence due to actin polymerization was recorded over 800 s using a PTI QM-4 QuantaMaster fluorimeter (excitation, 350 nm; emission, 407 nm; BRS). In actin depolymerization assays, pyrene-labeled actin (4 μM, 30% pyrene labeled) was copolymerized with increasing concentrations of MLP (0 to 10 μM) in F buffer. Depolymerization was induced by diluting samples to a final actin concentration of 0.2 μM in G buffer, and the subsequent decrease in pyrene fluorescence was recorded over 200 s. Experiments were conducted both under the above-described standard conditions and with additional combinations of free [Ca^{2+}] (0.01 μM and 300 μM) and pH (6.2, 6.8, and 7.4) conditions. Free [Ca^{2+}] and pH were adjusted to the desired value using MES, PIPES, Tris, EGTA, and/or $CaCl_2$ according to Table S2 in the supplemental material. When appropriate, dilution buffer was supplemented with 2 μM CFL1 (Cytoskeleton) or CFL2.

Cellular imaging. Confocal microscopy images were captured using a Zeiss LSM510 Meta laser scanning confocal microscope equipped with a ×63/1.4-numerical-aperture (NA) oil immersion Plan Apochromat objective in multitrack mode. Cerulean, GFP and Alexa Fluor 488, and Ve-

nus, respectively, were excited with a 458-nm, 488-nm, and 514-nm line of an argon laser; emitted light was collected with band-pass (BP) filters with widths of 470 to 500 nm, 505 to 550 nm, and 530 to 600 nm, respectively. Rhodamine phalloidin, Acti-stain 555 phalloidin, and Alexa Fluor 568 were excited using the 543-nm helium neon laser line, and emitted light was collected by a 560- to 615-nm BP filter. Acti-stain 670 and Alexa Fluor 633 were excited with the 633-nm helium neon laser line, and emitted light was collected by a 650-nm long-pass filter.

C2C12 cells were fixed for 20 min at 25°C with 3% formaldehyde (Agar Scientific) in phosphate-buffered saline (PBS) and permeabilized for 10 min with 0.5% Triton X-100 (Sigma) in PBS. The actin cytoskeleton was labeled with Acti-stain 555 or 670 phalloidin (Cytoskeleton). One-micrometer-thick optical sections through the nucleus or containing stress fibers were acquired. For three-dimensional (3D) pictures, stacks of 0.4-μm optical sections were generated and, if necessary, processed for deconvolution using Huygens essential software (SVI, Netherlands) to enhance the signal-to-noise ratio. For immunostaining, cells were labeled with primary antibodies (including anti-CRP3/MLP clone A-5 [Santa Cruz], antihemagglutinin [anti-HA] clone HA-7 [Sigma], anti-Myc [Abcam], and anti-sarcomeric α-actinin [Sigma]) in 0.5% BSA and subsequently labeled with secondary antibodies from the Alexa series (GAM-488, GAM-633, GAM-568, and GAR-568; Molecular Probes). Following washing, cells were mounted in Citifluor (Agar Scientific) on coverslips, sealed with nail polish, and examined by confocal microscopy.

BiFC. C2C12 or HL-1 cells were cotransfected with 2 μg of each bimolecular fluorescence complementation (BiFC) pair construct and 2 μg pFlag-Cerulean (transfection control) and prepared for cell imaging as previously described. For BiFC quantitative analyses, epifluorescence images were captured using a monochromatic camera (AxioCam HRm; Zeiss) with a combination of two filters for cyan and yellow fluorochromes (filter set 51, excitation, 458/10; BP 485/30; and filter set 53, excitation, 514/10; BP 575/50). Acquisition time was set to 25 ms for Cerulean and 800 ms for Venus. The BiFC efficiency of each BiFC pair tested was determined by quantifying fluorescence intensity in the Venus channel and normalization to the Cerulean signal. Data correspond to 3 independent experiments, including 50 cells each, and are expressed as the means of BiFC efficiency. Since the number of averaged measurements was higher than 100, the mean values were compared by *t* test using the R/Bioconductor software program. In addition, a corresponding box plot was generated to show the distribution of individual BiFC efficiency values.

Skewness analyses. C2C12 cells transfected with vectors allowing the expression of MLP-GFP, GFP only (control), or untagged MLP or with an empty vector (control) were stained with Acti-stain 555 phalloidin (Cytoskeleton). To control its expression and localization, untagged MLP was immunolocalized using a mouse anti-CRP3/MLP monoclonal antibody and an Alexa Fluor 488–goat anti-mouse secondary antibody. Fluorescent-phalloidin-labeled actin stress fibers were imaged by confocal microscopy using optimized (to avoid signal saturation) and identical settings for all analyzed cells. The skewness of signal intensity distribution of AF pixels in a 13- by 13-μm region of interest (ROI) was calculated using the software plug-in Kbi_Filter2d (ThinLine), developed by Higaki and coworkers (36) (available at http://hasezawa.ib.k.u-tokyo.ac.jp/zp/Kbi/HigStomata). Three independent experiments, including at least 20 measurements, were conducted for each transfection condition ($n \geq 60$). The normality of skewness values was validated by the Shapiro-Wilk test (41). Skewness average values were compared by *t* test, and a box plot was generated to show the distribution of skewness values using the R/Bioconductor software program.

For *in vitro*-reconstituted bundling assays conducted with MLP variants (see Fig. 7D and E), skewness average values were calculated from two independent experiments, each including at least 50 total internal reflection fluorescence microscopy (TIRFM) images acquired 40 min after the loading of the copolymerization mixture in the visualization chamber (see "TIRFM," below, for details).

Dual-labeling fluorescence microscopy assays. To determine AF relative orientation in MLP-induced bundles, we used a dual-labeling fluorescence assay similar to that described by Harris and coworkers (42). In brief, 1 μM actin was polymerized for 10 min in the presence of 3 μM MLP or 250 nM fascin in F buffer. Samples were subsequently labeled for 5 min with 1 μM Alexa Fluor 488-phalloidin (Molecular Probes), washed in F buffer to remove unbound fluorescent phalloidin, and centrifuged at 55,000 × *g* for 5 min to concentrate MLP-induced bundles. Elongation was resumed for an additional 15-min period in F buffer and in the presence of 1 μM actin monomer, 4 μM profilin, 3 μM MLP (or 250 nM fascin), and Alexa Fluor 568-phalloidin (Molecular Probes). Finally, bundles were diluted in 2 volumes of F buffer supplemented with 100 mM DTT, 0.5% methylcellulose, 20 μg/ml catalase, 100 μg/ml glucose oxidase, and 15 mM glucose, mounted on poly-L-lysine-coated slides, and imaged by confocal microscopy. Two independent experiments including 25 bundles each were performed.

TIRFM. Actin polymerization and bundle assembly were analyzed by TIRFM using a Zeiss Axiovert 200M inverted microscope equipped with a ×100/1.46-NA Alpha Plan-Apochromat TIRF objective. A 1:1 mixture of cold and Alexa Fluor 488-labeled actin (1 μM; Invitrogen) with 3 μM MLP or 250 nM fascin was prepared in fluorescence buffer (100 mM DTT, 0.5% methylcellulose, 20 μg/ml catalase, 100 μg/ml glucose oxidase, and 15 mM glucose) supplemented with 1× standard polymerization F buffer (50 mM KCl, 1 mM $MgCl_2$, 1 mM EGTA, and 10 mM imidazole, pH 7.0), flowed into a visualization chamber coated with 2.5 nM *N*-ethylmaleimide (NEM)–myosin (43), and immediately imaged. An excitation ray (488 nm) was provided by an argon laser, and emission light was collected with a 525/50 BP filter. Time-lapse images were acquired at 5-s intervals over 25 min with a Zeiss Axiocam HRm camera. Typical exposure time was 700 ms with a 5% laser filter. Images were analyzed using the ImageJ software program. When necessary, *xy* drift during time-lapse acquisition was corrected using the TurboReg plug-in (http://bigwww.epfl.ch/thevenaz/turboreg/). Kymographs were built along actin bundles using the MultiKymograph plug-in (http://www.embl.de/eamnet/html/body_kymograph.html).

RESULTS

MLP binds to, stabilizes, and cross-links actin filaments independently of calcium and pH. The ability of human MLP to directly bind to AFs and modify AF organization and dynamics was assessed in a series of *in vitro* assays. It is worth noting that the GST tag used to purify bacterially expressed MLP was cleaved off before subsequent analyses in order to exclude any potential artifacts due to GST dimerization. In binding (high-speed cosedimentation) assays, increasing amounts of MLP were incubated with polymerized AFs from rabbit skeletal muscle and subsequently centrifuged at 100,000 × *g*. The resulting pellet and supernatant fractions were analyzed by SDS-PAGE. As shown in Fig. 1A, MLP accumulated in the pellet together with AFs (two lower panels), whereas it mostly remained in the supernatant in the absence of AFs (two upper panels). From three independent experiments, we calculated an apparent equilibrium dissociation constant (K_d) of 1.18 ± 0.27 μM and an MLP-to-actin ratio at saturation of 1.56 ± 0.22 (Fig. 1B). Similar data were obtained using other commercially available sources of actin, including chicken gizzard smooth muscle, human platelet nonmuscle, and bovine cardiac muscle actin (Cytoskeleton), indicating that MLP has no selectivity for actin isoforms (data not shown).

Pyrene-actin assays revealed that MLP does not modify the rate of actin polymerization (see Fig. S4A in the supplemental material). In contrast, MLP stabilized AFs against dilution-mediated depolymerization in a concentration-dependent manner (Fig. 1C). Full AF stabilization occurred at MLP/actin molar ratios of >1:1. Since MLP was recently shown to colocalize with cofilin 2

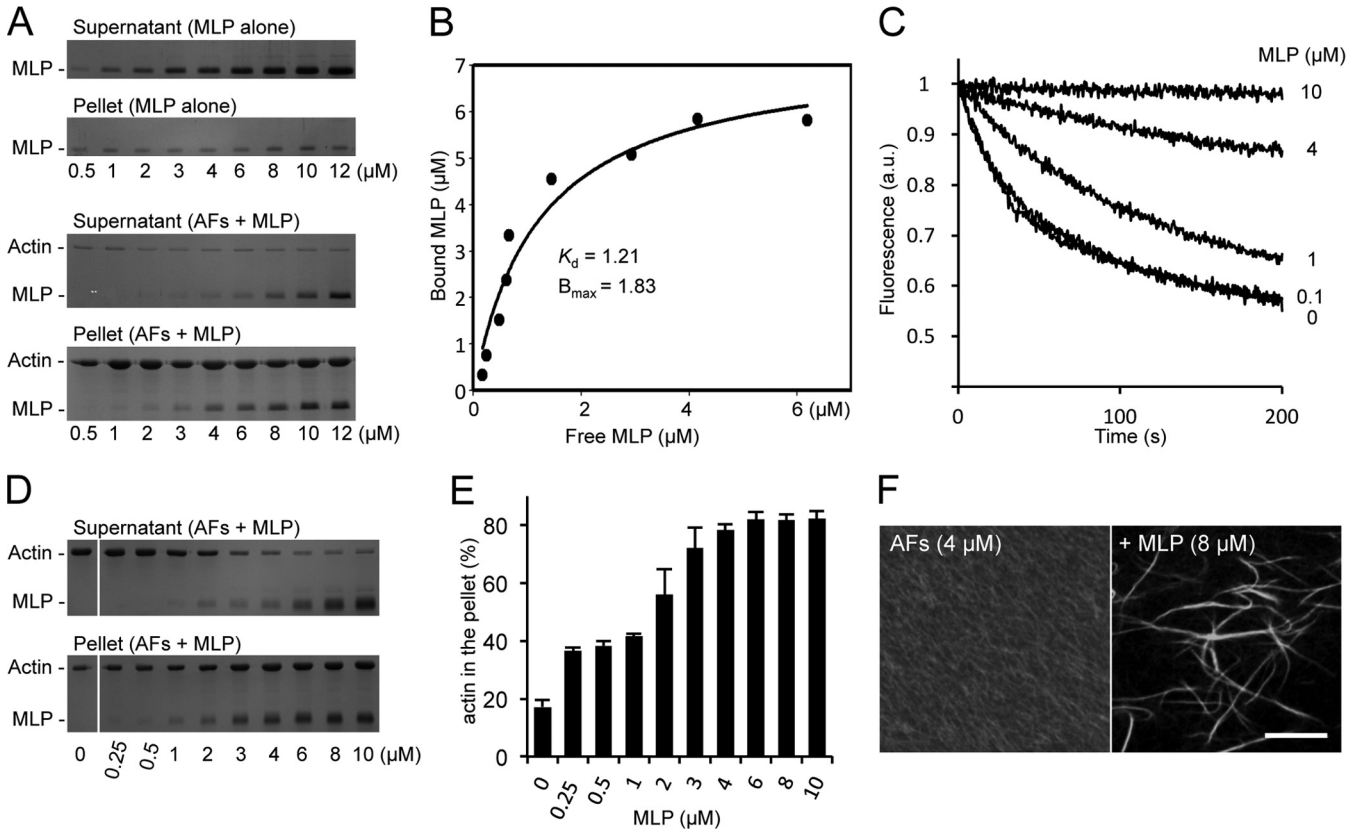

FIG 1 MLP directly binds to, stabilizes, and bundles actin filaments. (A) High-speed cosedimentation assay. After centrifugation at 100,000 × *g*, MLP accumulates in the pellet fraction in the presence of actin filaments (4 μM; two lower gel panels) but not in the absence of AFs (two upper gel panels). (B) Apparent equilibrium dissociation constant (K_d) determined from the high-speed cosedimentation experiments shown in panel A. The amount of MLP present in the pellet and the supernatant was quantified, and the concentration of F-actin-bound protein was plotted against the concentration of free protein. Experimental data were fitted with a hyperbolic function from which K_d and maximal binding capacity (B_{max}) values were deduced. (C) Depolymerization assay. Pyrene-labeled actin filaments (4 μM) were copolymerized with increasing amounts of MLP (0 to 10 μM) and induced to depolymerize by a 10-fold dilution. Initial fluorescence was set to 1. (D) Low-speed cosedimentation assay. After centrifugation at 12,000 × *g*, actin filaments (4 μM) sediment in an MLP concentration-dependent manner (0.25 to 10 μM). (E) Quantification of three independent experiments as shown in panel D. Results are expressed as the percentages of total actin in the pellet as a function of MLP concentration (error bars indicate SD; $n = 3$). (F) Direct visualization of actin bundles induced by MLP after Alexa Fluor 488–phalloidin staining. Bar = 10 μm.

(CFL2) at the sarcomeric Z line of human striated muscles and to directly interact with CFL2 *in vitro* (44), additional pyrene-actin depolymerization assays were conducted in the presence of CFL1 or CFL2. Results indicate that MLP strongly reduces the ability of CFL1 and CFL2 to enhance actin depolymerization, supporting that MLP protects AF from depolymerization (see Fig. S4B and C). In contrast to the findings of Papalouka et al. (44), who reported that at specific MLP/cofilin ratios MLP enhances CFL2 depolymerizing activity, our data support that CFL2 and MLP have opposite effects on AF dynamics irrespective of their relative concentrations.

Low-speed cosedimentation assays revealed that MLP promotes the formation of higher-order actin structures that sediment at 12,000 × *g* (Fig. 1D and E). Fluorescence microscopy identified these structures as bundles of AFs, indicating that MLP functions as an actin-bundling protein *in vitro* (Fig. 1F).

Calcium concentration and pH play critical roles and can undergo significant fluctuations during muscle activity. Since both factors regulate the activities of many actin-binding proteins, we investigated whether they influence MLP activity. To do so, we conducted pyrene-actin depolymerization assays using diverse combinations of free [Ca^{2+}] (0.01 μM and 300 μM) and pH (6.2, 6.8, and 7.4). The data indicate that MLP stabilizes AFs with very similar efficacies under all conditions tested (see Fig. S5A in the supplemental material). In contrast, the stabilizing activity of a plant-related LIM protein that was previously shown to respond to calcium and pH, namely, *Arabidopsis* AtPLIM2c (37), was severely downregulated upon an increase of [Ca^{2+}] and/or pH (see Fig. S5B). Consistent with these data, MLP induced low-speed AF sedimentation irrespective of [Ca^{2+}] and pH conditions, whereas AtPLIM2c was active only at low [Ca^{2+}] and pH (see Fig. S5C and D, respectively). In conclusion, MLP displays AF-binding, -stabilizing, and -bundling activities, and these activities are not directly regulated by calcium and pH.

MLP-GFP associates with the actin cytoskeleton and promotes actin bundling in diverse cell types. The actin regulatory activities of MLP were first investigated with undifferentiated C2C12 skeletal myoblasts in which endogenous MLP is not expressed (1). C2C12 cells were transiently transfected with a construct encoding MLP fused at its C terminus to GFP (MLP-GFP). As shown by F-actin colabeling (Acti-stain 555 phalloidin), MLP localized mainly along actin stress fibers (Fig. 2A to C). Diffuse

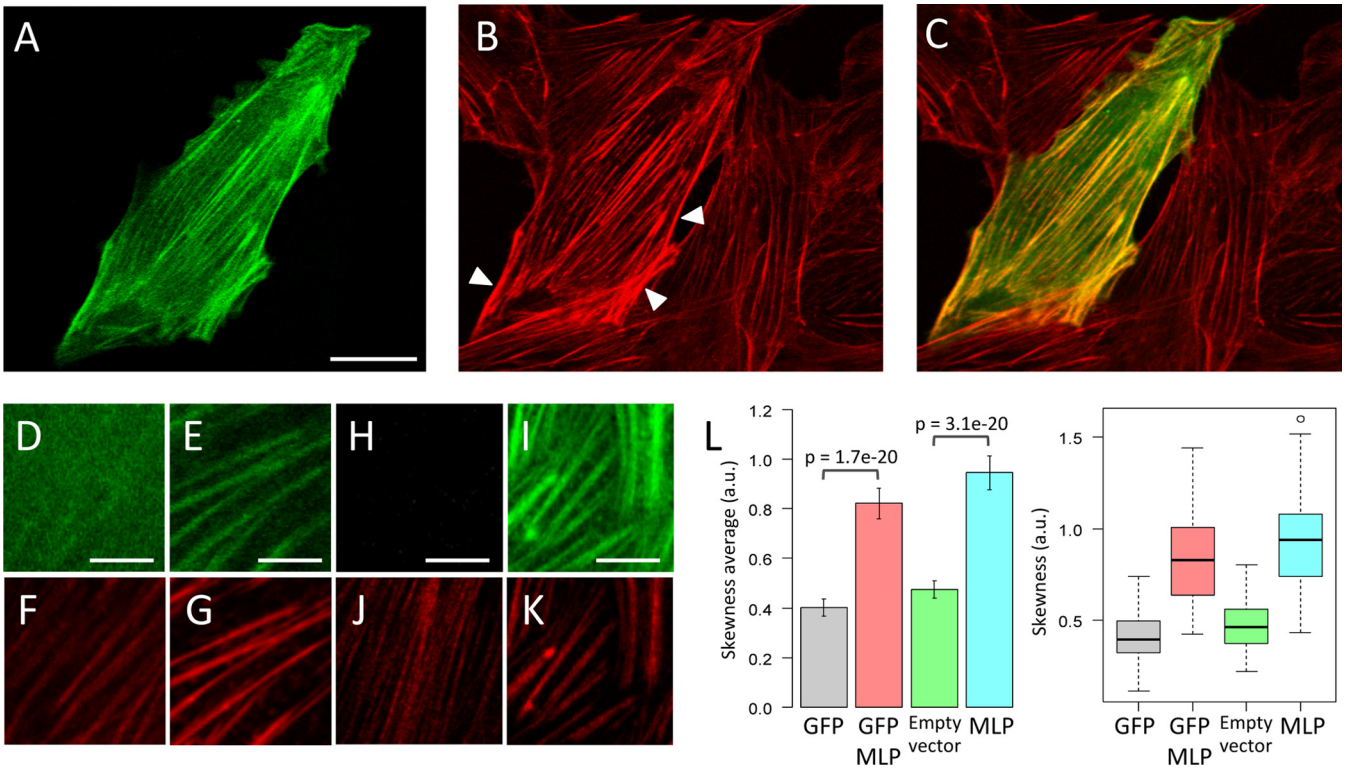

FIG 2 MLP promotes actin bundling in C2C12 cells. (A) Subcellular distribution of MLP-GFP in transfected C2C12 cells. (B) Actin cytoskeleton organization (as visualized by Acti-stain 555 phalloidin staining) in the MLP-GFP-expressing cell shown in panel A and in the surrounding, nontransfected cells. Arrowheads indicate very thick actin stress fibers in the MLP-GFP-expressing cell. (C) Merged image of panels A and B. (D to K) Examples of ROI (13 by 13 μm) used for skewness measurements in Acti-stain 555 phalloidin-stained cells transfected with GFP only (D and F), MLP-GFP (E and G), empty vector (H and J), or untagged MLP (I and K). Both the green (D, E, H, and I) and the red (F, G, J, and K) channels are shown. For empty vector- and untagged MLP-transfected cells, MLP was immunolocalized using an anti-MLP antibody (H and I). (L) The left chart shows the skewness average calculated for each transfection condition from three independent experiments ($n \geq 60$). Error bars denote 95% confidence intervals. Some *t* test *P* values are indicated. The right chart shows the corresponding box plot depicting the distribution of skewness values. Bars = 20 μm (A to C) or 4 μm (D to K).

cytoplasmic and nuclear fluorescent signals were also observed in most transfected cells. Similar data were obtained when GFP was fused to the N-terminal extremity of MLP (data not shown). Noticeably, MLP-GFP-expressing cells exhibited thicker actin stress fibers than the surrounding nontransfected cells (Fig. 2B). Such an observation is consistent with the above-characterized MLP actin-bundling activity. However, the interpretation of cellular data is complicated by the presence of MLP cytoskeletal partners that can potentially mask/interfere with the direct effects of MLP on the actin cytoskeleton. To address this question, we ectopically expressed GFP-fused MLP in plant cells. Noticeably, mammalian and plant actins are highly conserved, with more than 90% amino acid identity, and there is no equivalent to the main cytoskeletal partners of MLP, including α-actinin, zyxin, and telethonin (T-CAP), in plant genome/proteome databases. Accordingly, plant cells represent a useful experimental system for confirming the autonomous actin-binding and -bundling activities of human MLP. As shown in Fig. S6A to D in the supplemental material, MLP-GFP decorated the actin cytoskeleton of tobacco BY2 cells. Similar results were obtained with an N-terminally fused GFP construct (GFP-MLP) (see Fig. S6E). In contrast, GFP alone exhibited only a diffuse cytosolic distribution (data not shown). Remarkably, MLP-labeled bundles (see Fig. S6D and E) were substantially thicker than those labeled with the fimbrin-derived fusion protein YFP-fABD2 (see Fig. S6F), a reliable actin marker widely used in plants (45). These data therefore support that MLP binds to AFs and promotes actin bundling independently of its cytoskeletal partners.

To confirm MLP actin-bundling activity in C2C12 cells by a quantitative and statistically relevant method, MLP-GFP- and "GFP only"-expressing cells (control) were labeled with Acti-stain 555 phalloidin and subjected to confocal microscopy analysis using identical acquisition parameters. Thick optical sections comprising stress fibers on their whole thickness were skeletonized, and the skewness of the red fluorescence intensity distribution (a reliable indicator of actin bundling) was calculated, following the procedure described by Higaki and coworkers (36). As shown in Fig. 2D to G and L, MLP-GFP increased the skewness value by a factor 2 compared to results with GFP alone, confirming the previously noticed increase of stress fiber thickness. Importantly, a similar shift of skewness was induced by an untagged version of MLP (Fig. 2H to L).

Endogenous MLP is expressed predominantly in differentiated cardiac muscle cells (1). We thus extended the above data by expressing MLP-GFP in the HL-1 cardiac muscle cell line developed by Claycomb and coworkers (39, 46). This cell line was shown to retain a differentiated cardiac phenotype as well as the ability to spontaneously beat. Beside its diffuse cytoplasmic distribution, MLP-GFP decorated sarcomeric structures and colocalized with AFs (Fig. 3A to C). In addition, MLP-GFP colocalized with α-ac-

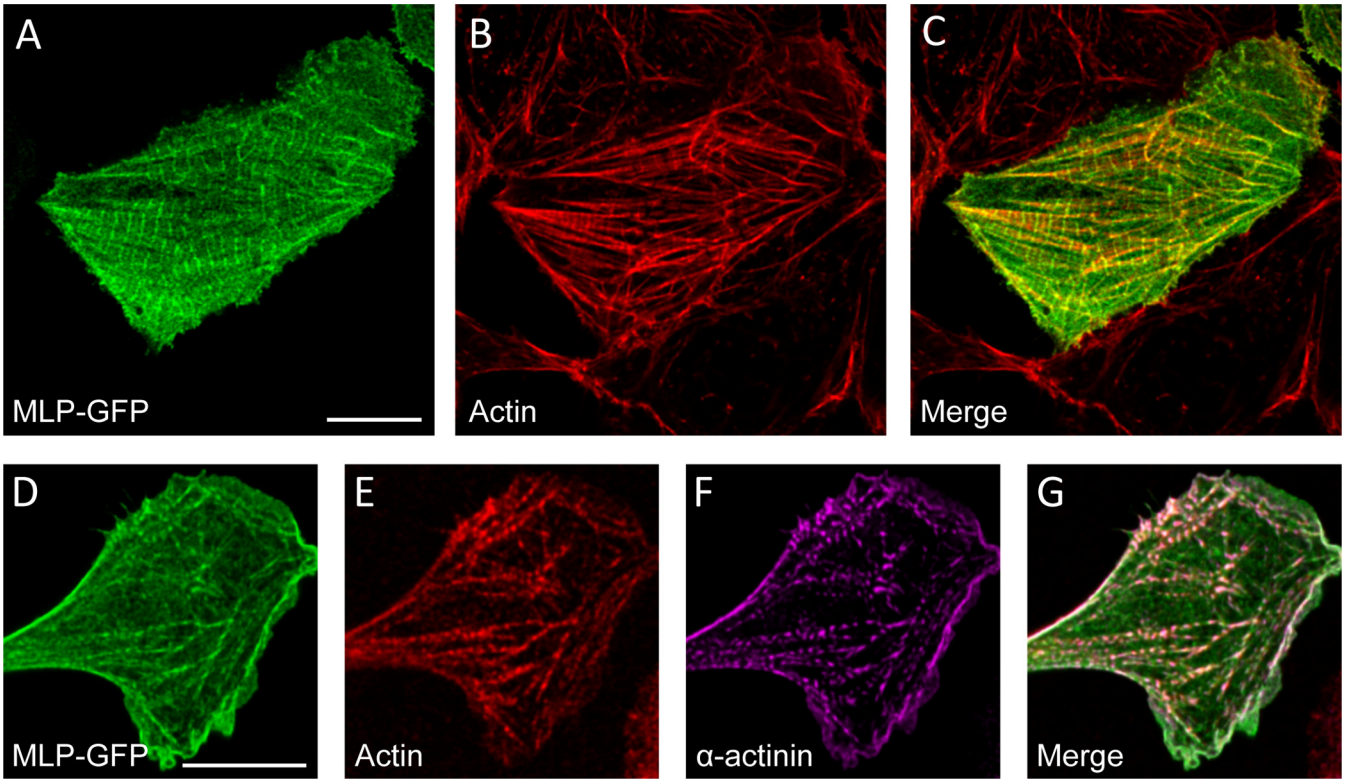

FIG 3 MLP localizes to sarcomeric structures in HL-1 cardiac muscle cells. (A) Subcellular distribution of MLP-GFP in transfected HL-1 cells. (B) Actin cytoskeleton organization in the MLP-GFP-expressing cell shown in panel A and in the surrounding, nontransfected cells. (C) Merged image of panels A and B. (D to G) Colocalization of MLP and alpha-actinin in nascent myofibrils. Actin cytoskeleton (E) or immunolocalized sarcomeric α-actinin (F) in one MLP-GFP-expressing HL-1 cell (D) is shown. The corresponding merged image is shown in panel G. Bars = 10 μm.

tinin in nascent myofibrils (Fig. 3D to G), an observation that is well consistent with the previously reported localization of endogenous MLP at the Z line of muscle cells (18, 24, 44, 47). In support of MLP also functioning as an actin cross-linker/stabilizer in differentiated muscle cells/tissues, MLP-GFP-expressing HL-1 cells frequently exhibited more prominent actin-based structures than the surrounding nontransfected cells (Fig. 3B).

MLP cross-links actin filaments in unipolar and mixed-polarity bundles. To characterize the properties of MLP-induced bundles, AFs were polymerized in the presence of MLP and imaged by real-time total internal reflection fluorescence (TIRF) microscopy. In the course of their polymerization, AFs assembled into long and thick bundles resembling those produced by the bundling protein fascin (Fig. 4A to C; see also Movie S7 in the supplemental material). However, the bundles induced by MLP (Fig. 4B) had a wavier appearance and formed more reticulated networks than those induced by fascin (Fig. 4C), suggesting mechanistic differences between the two actin-bundling proteins. We then investigated how MLP-induced bundles assemble and grow. Most frequently, the elongating extremity of one filament contacted the side of another filament or bundle and continued to grow while remaining associated with this filament/bundle (Fig. 4D; see also Movie S8). In some other cases, the two filaments/bundles fused over a long distance by a zippering mechanism (Fig. 4E; see also Movie S9) that has previously been described for other cross-linking proteins, including villins (48) and one plant formin (49).

The relative orientation of AFs within MLP-induced bundles was determined by following the fast-growing barbed end of individual AFs. Some MLP-induced bundles exclusively contained AFs of identical polarity (Fig. 4F and H; see also Movie S10 in the supplemental material), whereas others contained AFs of opposite polarities (Fig. 4G and I; see also Movie S10). This strikingly contrasted with bundles induced by fascin, which exclusively exhibited AFs elongating in the same direction (data not shown). The polarity of MLP- and fascin-induced bundles was further analyzed in a dual-fluorescence microscopy assay (42). AFs were copolymerized with MLP or fascin, and the resulting bundles were stabilized and stained with Alexa Fluor 488 phalloidin (green). Then, polymerization was resumed by the addition of profilin-bound actin monomers (1 μM actin and 4 μM profilin). Under such conditions, the elongation at the AF pointed end was strongly reduced, whereas barbed ends could efficiently polymerize. Alexa Fluor 568 phalloidin (red) was used to label the newly grown sections of AFs. In good agreement with TIRFM data, about 50% of MLP-induced bundles resumed growth at both extremities (Fig. 4J to L), whereas the remaining 50% exclusively reelongated at only one extremity (Fig. 4M to O). In contrast, the vast majority (>90%) of fascin-induced bundles reelongated at only one extremity (Fig. 4P to R). In conclusion, MLP exhibits no intrinsic selectivity for AF polarity and, contrary to the case with fascin, can promote the formation of mixed-polarity bundles.

MLP self-associates along the filamentous actin cytoskeleton. Some AF cross-linkers, e.g., α-actinin, require dimerization

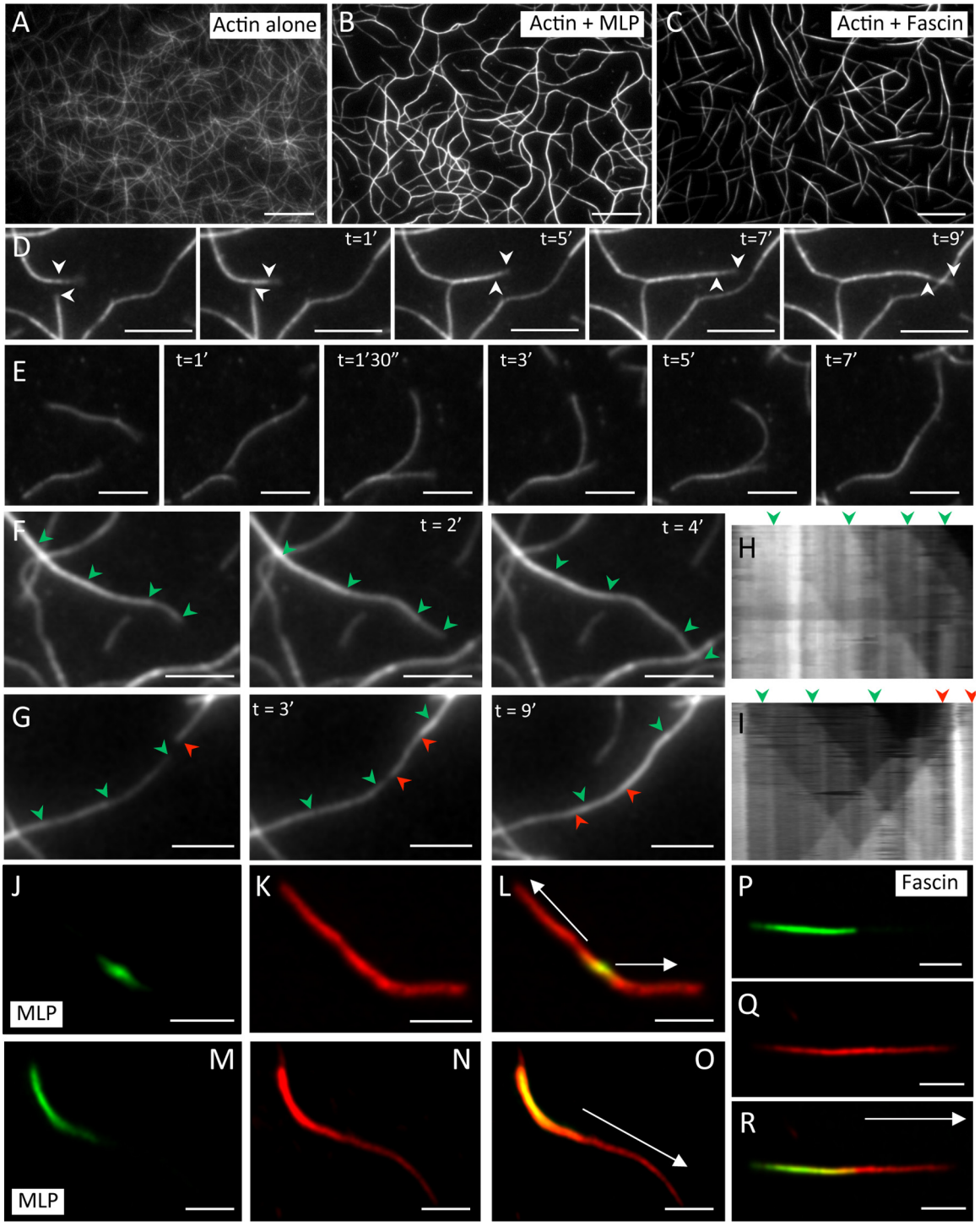

FIG 4 MLP-induced actin bundling in reconstituted assays. (A to C) Actin filament network after 18 min of polymerization of 1 μM actin alone (A) or with 3 μM MLP (B) or 250 nM fascin (C). (D and E) Typical examples of actin bundling induced by MLP. (F and G) Typical examples of unipolar (F) or mixed-polarity (G) bundles induced by MLP. (H and I) Ten-minute kymographs corresponding to the bundles shown in panels F and G, respectively. (J to R) Dual-fluorescence labeling assays showing that MLP induces both mixed-polarity (J to L) and unipolar (M to O) bundles, whereas fascin exclusively induces unipolar bundles (P to R). Arrows indicate the newly grown actin bundle sections (in red) after addition of profilin-bound actin monomers (1 μM actin, 4 μM profilin) and Alexa Fluor 568-phalloidin staining. Arrowheads in panels D and F to I indicate the fast-growing end of actin filaments. Bars = 10 μm (A to C), 5 μm (D), 3 μm (E and F), or 2 μm (J to R).

to cross-link AFs. Using subcellular fractionation followed by Western blotting under nondenaturing conditions, Boateng and coworkers (22) have previously reported the presence of endogenous MLP di- and oligomers in membrane and cytoskeletal fractions of myocytes. Interestingly, MLP was detected mostly as a monomer in the nuclear fraction. From these data and the here-characterized MLP actin-binding and -bundling activities, we anticipated that MLP self-associates along the filamentous actin cy-

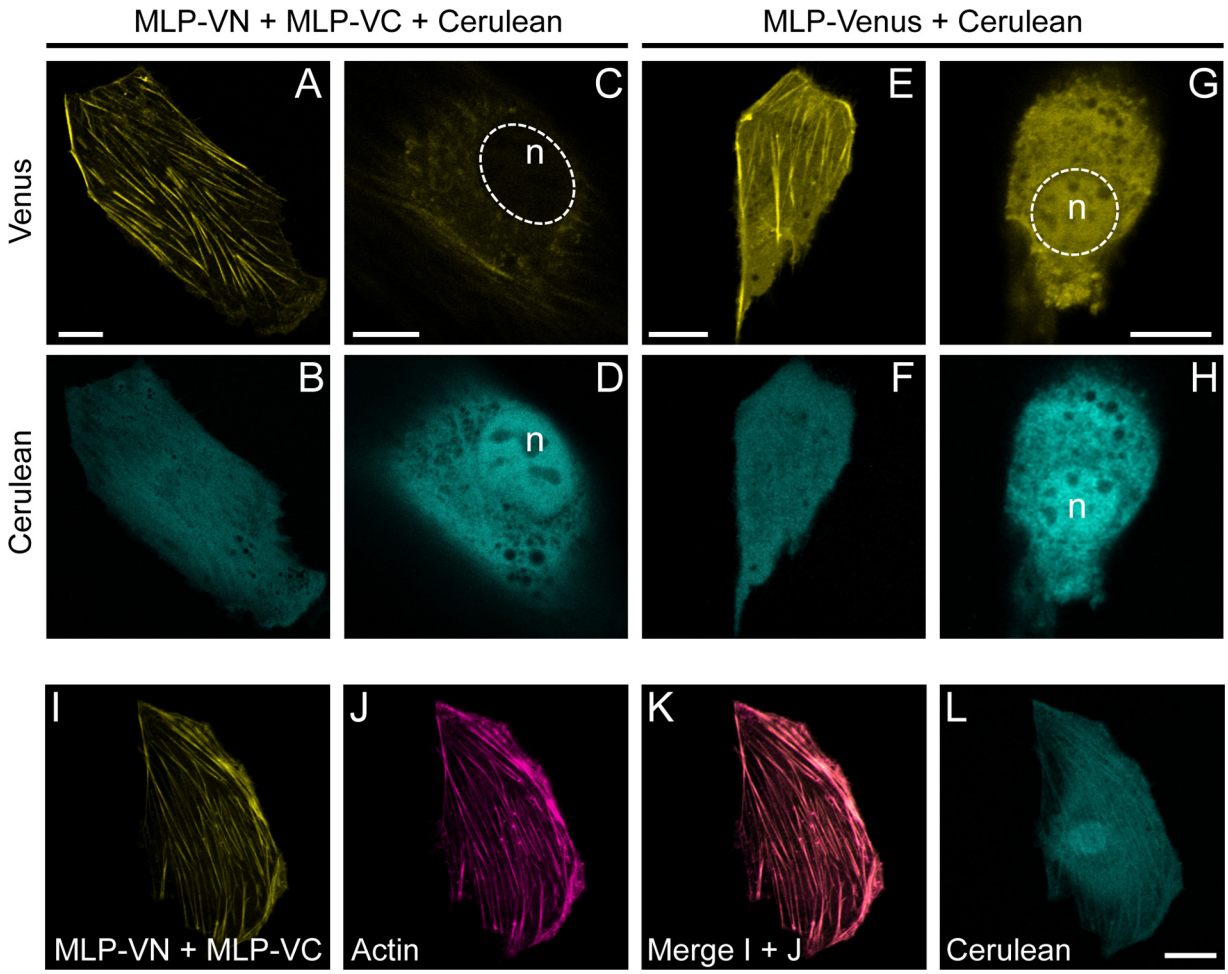

FIG 5 MLP BiFC complexes localize along the actin cytoskeleton. (A and C) Typical BiFC signal in actin stress fiber-containing (A) or nucleus-containing (C) optical sections of C2C12 cells following cotransfection with Cerulean and BiFC vectors encoding MLP fused via its C terminus to N-terminal (MLP-VN) and C-terminal (MLP-VC) fragments of Venus, respectively. (E and G) Typical localization of full-length Venus-fused MLP (MLP-Venus) in actin stress fiber-containing (E) or nucleus-containing (G) optical sections of C2C12 cells. (B, D, F, and H) Cerulean signal (used as a transfection and expression-level control) in the cell regions shown in panels A, C, E, and G, respectively. Note that panels A to D and E to H were acquired using identical acquisition settings. (I to L) Colocalization of MLP BiFC complexes with the actin cytoskeleton following Acti-stain 670 phalloidin staining. (K) Merged image of panels I and K. (L) Cerulean transfection control. n, nucleus. Bars = 10 μm.

toskeleton to promote actin bundling. However, the precise subcellular distribution of MLP complexes in individual, intact and living cells has not been reported so far. To do so, we conducted bimolecular fluorescence complementation (BiFC) experiments (50). Plasmid vectors encoding MLP fused by its C terminus to N-terminal or C-terminal fragments of the fast-maturing YFP variant Venus (MLP-VN155 and MLP-VC155, respectively) were cotransfected in myogenic C2C12 cells. A third plasmid, encoding the fluorescent protein Cerulean (51), was used as a transfection control. It is noteworthy that we used an improved version of Venus containing the I152L mutation, which was recently shown to dramatically reduce self-assembly between the Venus N- and C-terminal fragments and to increase the signal-to-noise ratio of the BiFC assay (52). Western blotting using an anti-human MLP antibody confirmed the expression of the BiFC constructs with the expected molecular weights and with similar levels (data not shown). Confocal microscopy analyses revealed that Cerulean-expressing cells exhibited strong Venus fluorescence, indicating the formation of BiFC complexes (Fig. 5A to D). Remarkably, cells exhibited a prominent BiFC signal along their actin stress fibers (Fig. 5A and I to L), whereas the fluorescence was much weaker in the rest of the cytoplasm and the nuclear compartment (Fig. 5C). This contrasted with the substantial diffuse signal observed in the cytosol and nucleus of control cells expressing MLP fused to full-length Venus (MLP-Venus) (Fig. 5E to H). The presence of MLP BiFC complexes along actin stress fibers was confirmed using combinations of N-terminally and C-terminally fused Venus fragments (VN155-MLP and MLP-VC155; MLP-VN155 and VC155-MLP) or exclusively N-terminally fused Venus fragments (VN155-MLP and VC155-MLP; see Fig. S11 in the supplemental material). We noticed, however, that compared to the sharp and strong actin cytoskeleton decoration observed with the C-terminally fused MLP BiFC pair, most cells exhibited overall lower fluorescence intensity. In addition, they showed nonnegligible cytosolic and nuclear fractions of fluorescence. Nevertheless, the BiFC signal was always highest along stress fibers, supporting that MLP complexes preferentially form and/or localize along the actin cytoskeleton. MLP self-association was confirmed in differ-

entiated cardiac muscle HL-1 cells (see Fig. S12A and B in the supplemental material). As seen in C2C12 cells, the BiFC signal concentrated mostly on AF-containing structures, including those labeled by α-actinin (see Fig. S12E to H).

MLP self-associates via its N-terminal LIM domain. Since LIM domains function primarily as protein interaction domains (11, 53), we evaluated their role in MLP self-association and bundling activity. We generated additional BiFC vectors allowing the expression of MLP mutants lacking either the first LIM domain (LIM1), the second LIM domain (LIM2), or a section of the C-terminal domain (Ct) (control) fused to the Venus C-terminal fragment (MLPΔLIM1-VC155, MLPΔLIM2-VC155, and MLPΔCt-VC155, respectively; see Fig. S3 in the supplemental material). Each of these vectors was coexpressed in C2C12 cells with the complementary full-length MLP BiFC construct (MLP-VN155) and Cerulean (to normalize the transfection and protein expression levels; Fig. 6A to D). Both Venus and Cerulean signals were quantified, and the BiFC efficiency (Venus-to-Cerulean ratio) for each BiFC pair was calculated and compared to the BiFC efficiency obtained for the reference BiFC pair MLP-VN155/MLP-VC155 (Fig. 6F). From three independent experiments, we determined a BiFC efficiency of 0.96 ± 0.09 for the reference BiFC pair. In striking contrast, the MLP-VN155/MLPΔLIM1-VC155 pair generated a BiFC efficiency of only 0.21 ± 0.04 (Fig. 6B and F). Moreover, when LIM1 was deleted from both complementary BiFC constructs (i.e., MLPΔLIM1-VN155/MLPΔLIM1-VC155), Venus complementation was virtually abolished, with a BiFC efficiency of 0.05 ± 0.01 (Fig. 6F). As exemplified in Fig. 6E, the expression of complementary BiFC constructs was systematically controlled using immunocytochemistry. We therefore concluded that LIM1 plays a critical role in MLP self-association. No substantial modification in BiFC efficiency was noticed for the control BiFC pair MLPΔCt-VC155/MLP-VN155 (1.11 ± 0.16), supporting that the C-terminal domain is dispensable for MLP self-interaction (Fig. 6D and F). Interestingly, we observed a moderate yet significant reduction in BiFC efficiency (0.74 ± 0.09) for the BiFC pair MLPΔLIM2-VC155/MLP-VN155 (Fig. 6C and F). Although the BiFC efficiency further decreased when LIM2 was deleted from both complementary BiFC constructs (i.e., MLPΔLIM1-VN155/MLPΔLIM1-VC155), it remained much higher (about 8-fold) than the value calculated for the LIM1-deleted BiFC pair (i.e., 0.39 ± 0.07 versus 0.05 ± 0.01, respectively). In conclusion, MLP self-association is driven mainly by LIM1, whereas LIM2 has only a facilitating/enhancing role. Importantly, the prominent role of LIM1 in MLP self-association was validated in cardiac muscle HL-1 myocytes (see Fig. S12C and D).

MLP actin-bundling activity relies on both N- and C-terminal LIM domains. Contrary to the case with MLPΔLIM1 and MLPΔCt, MLPΔLIM2 failed to decorate the actin cytoskeleton in C2C12 cells (Fig. 6G to I). Thus, the moderate yet significant reduction in BiFC efficiency calculated for the BiFC pair MLP-VN155/MLPΔLIM2-VC155 (Fig. 6C and E) likely reflects that, contrary to the case with MLP, MLPΔLIM2 does not bind to the actin cytoskeleton, lowering the efficiency of BiFC complex formation at this location. In other terms, this suggests that AFs facilitate MLP self-association by bringing MLP monomers in close proximity (via LIM2-AF interaction) and thereby promoting their association (via LIM1-LIM1 interaction). It remained uncertain, however, if LIM2 functions as an intrinsic and direct actin-binding domain. To address this question, we conducted high-speed cosedimentation analyses with both MLPΔLIM1 and MLPΔLIM2. Contrary to the case of MLPΔLIM1, which retained substantial actin-binding activity (Fig. 7A), MLPΔLIM2 was unable to bind to and sediment with AFs (Fig. 7B). Surprisingly, used as single domains, neither LIM1 nor LIM2 could bind to AFs (Fig. 7C). Thus, although MLP binds directly to AFs via LIM2, the latter domain is not sufficient to trigger autonomous actin-binding activity. Consistent with the above data, MLPΔLIM2 was unable to induce the formation of actin bundles (Fig. 7D and E). More interestingly, MLPΔLIM1 could promote actin bundling, although with a strongly reduced efficiency compared to that of full-length MLP (Fig. 7D). Accordingly, using quantitative analyses, we calculated a skewness average value for MLPΔLIM1 which was >50% lower than the one obtained for full-length MLP (Fig. 7E). Noticeably, the bundles induced by MLPΔLIM1 were qualitatively dissimilar from those induced by full-length MLP, with a thinner and wavier appearance (Fig. 7D). We thus conclude that both LIM2 (actin-binding) and LIM1 (self-association) are required for MLP actin-bundling activity.

DISCUSSION

Based on its localization to various sarcomeric structures and its ability to shuttle to the nucleus in response to mechanical stress (22, 28, 29), MLP has been proposed to serve as a stress sensor and signaling molecule between myocyte compartments (26). Collectively, our data point to an additional role for MLP in the maintenance of cell cytoarchitecture, through direct regulation of actin cytoskeleton organization and dynamics. Indeed, we found that, like its relatives CRP1 and CRP2 (30, 32), MLP binds directly to AFs *in vitro* without the requirement of any other protein. In addition, it autonomously cross-links AFs into bundles and protects them from dilution- and cofilin-mediated depolymerization. Consistent with its intrinsic activities, MLP decorates the actin cytoskeleton and significantly increases the cellular actin-bundling level when transfected into C2C12 and HL-1 cells.

Supporting that MLP contributes to the maintenance of muscle cell integrity through an actin-based mechanism, endogenous MLP has repeatedly been localized at critical mechanical elements where AFs are anchored and cross-linked, including the Z disk and costamere (12, 18, 22, 24, 25, 27, 54). Moreover, the functional and structural cardiac alterations observed in mouse after MLP gene ablation (1, 18, 55) or substitution (knock-in) by a mutated version carrying a missense mutation (10T → C; W4R) identified in human patients with cardiomyopathy and heart failure (25) are reminiscent of a deficiency in AF cross-links, e.g., increased compliance, impaired resistance to mechanical stress, irregular cardiomyocyte shape, and disorganization of myofibrils. At the Z disk, AFs from adjoining sarcomeres are assumed to be primarily cross-linked by homodimers of α-actinin, the most abundant Z-disk component (56). However, a recent study has suggested that the MLP-related *Drosophila* protein Mlp84B has a function similar and complementary to that of α-actinin in muscle stabilization through the cross-linking of AFs at the Z-disk and muscle-membrane attachment sites (35). Although the biochemical activity of Mlp84B has not been directly assessed, the forced accumulation of Mlp84 in muscle nuclei induced the formation of actin cables independently of α-actinin, supporting that, like human MLP, Mlp84 is an autonomous AF-bundling protein. Interestingly, MLP and α-actinin physically interact (13, 35), and cardiomyo-

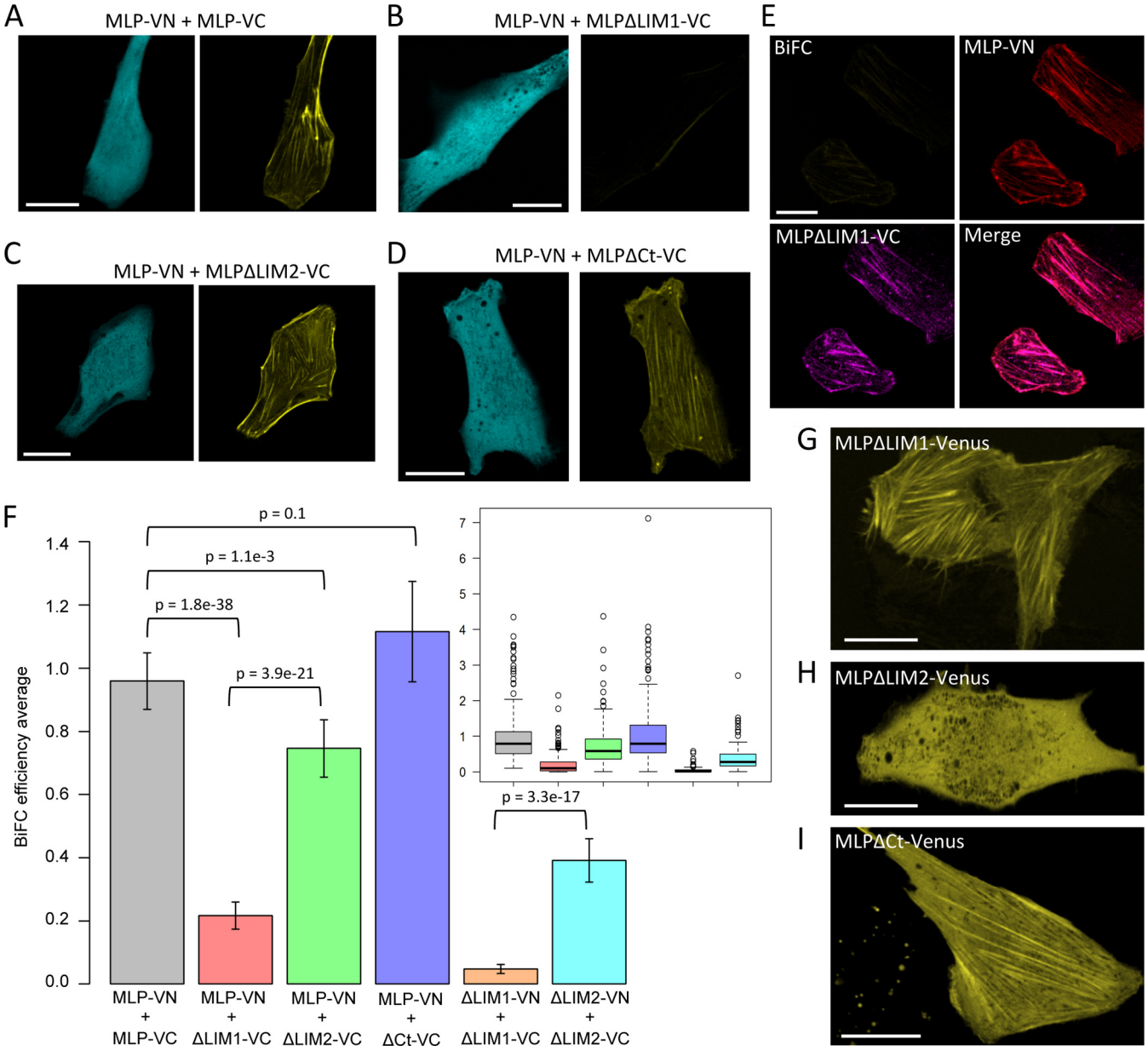

FIG 6 MLP self-association mainly relies on the N-terminal LIM domain. (A to D) Typical BiFC signal (right panels, yellow) in C2C12 cells transfected with the following BiFC pairs: MLP-VN plus MLP-VC (A), MLP-VN plus MLPΔLIM1-VC (B), MLP-VN plus MLPΔLIM2-VC (C) and MLP-VN plus MLPΔCt-VC (D). The left panels (blue) show Cerulean signals (used as transfection and expression-level controls for quantitative analyses). (E) Immunolocalization of MLP-VN (using anti-c-Myc antibodies) and MLPΔLIM1-VC (using anti-HA antibodies) in cotransfected C2C12 cells. Note that both BiFC constructs decorate actin stress fibers (see the "Merge" panel). (F) BiFC efficiency (Venus/Cerulean) average calculated from three independent experiments ($n \geq 125$) using the BiFC pairs shown in panels A to D and the two additional BiFC pairs MLPΔLIM1-VN plus MLPΔLIM1-VC and MLPΔLIM2-VN plus MLPΔLIM2-VC. Error bars denote 95% confidence intervals. Some *t* test *P* values are indicated. The inset shows a box plot depicting the distribution of the BiFC efficiency values calculated for each BiFC pair. (G to I) Typical subcellular distribution of full-length Venus-fused MLPΔLIM1 (G), MLPΔLIM2 (H), or MLPΔCt (I) in transfected C2C12 cells. Note that only MLPΔLIM2-Venus exhibits no AF colocalization. Bars = 20 μm.

cyte-associated mutations have been shown to disrupt their interaction (19, 57), pointing to a close functional link. Beside the colocalization of MLP and α-actinin in HL-1 cells (Fig. 3D to G; see also Fig. S12E to H in the supplemental material), our data point to additional and striking similarities between both proteins supporting that they coregulate AF stability. First, like cardiac α-actinin (58), MLP cross-links AFs irrespective of calcium concentration. This lack of calcium responsiveness is consistent with their (putative) role of AF stabilizers/cross-linkers during muscle activity. Second, contrary to selective AF cross-linkers, like fascin, which promote the formation of unipolar bundles (40, 59–61), both MLP and α-actinin (60, 62, 63) are able to generate mixed-polarity bundles. It is therefore conceivable that they cooperate at the Z disk to cross-link antiparallel AFs coming from adjoining sarcomeres.

Using subcellular fractionation followed by nonreducing

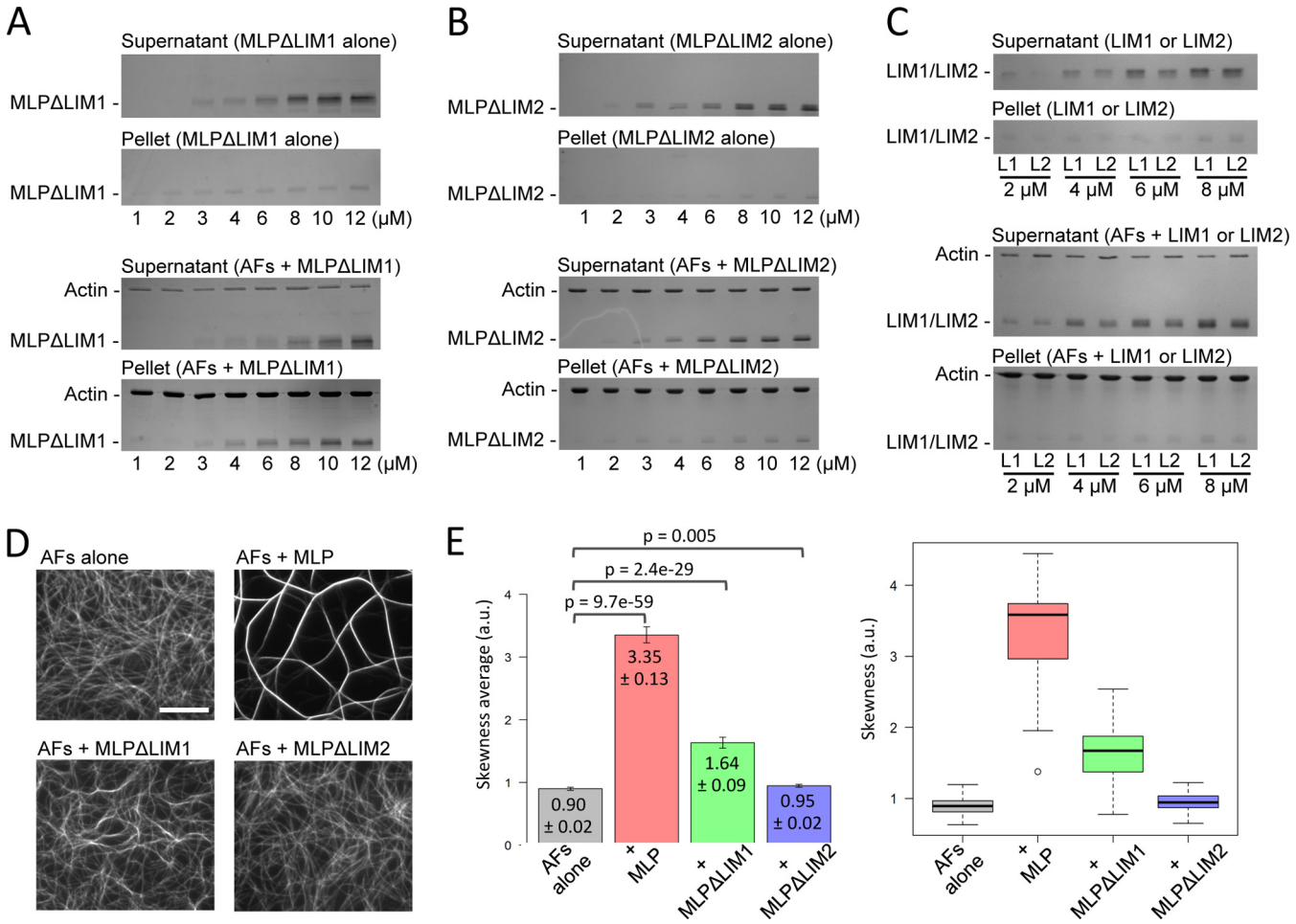

FIG 7 C-terminal LIM domain is necessary for actin-binding activity, and both N- and C-terminal LIM domains are required for optimal actin-bundling activity. (A to C) High-speed cosedimentation assays conducted with 4 μM AFs and MLPΔLIM1 (A), MLPΔLIM2 (B), or the individual LIM domains LIM1 and LIM2 (C). Note that although LIM2 is required for MLP actin-binding activity (B), it does not bind to AFs as an isolated domain (C). The upper gel panels show control experiments for each protein conducted in the absence of AFs. (D) Direct visualization using TIRFM of AFs (1 μM) alone or in the presence of MLP, MLPΔLIM1, or MLPΔLIM2 (3 μM). Bar = 10 μm. (E) Quantitative analysis of the actin-bundling activity of MLP, MLPΔLIM1 or MLPΔLIM2 using the skewness parameter. The left chart shows the skewness average calculated for each transfection condition from at least two independent experiments ($n \geq 85$). Error bars denote 95% confidence intervals. Skewness average values and some *t* test P values are indicated. The right chart shows the corresponding box plot depicting the distribution of skewness values.

Western analysis, Boateng and coworkers (22) previously established that endogenous MLP self-associates in the cytoplasm, while it remains mostly monomeric in the nuclear compartment. However, the roles of MLP complexes are not clear. Based on our data, we propose that one of these roles is the cross-linking/stabilization of AFs. First, our BiFC data indicate that MLP complexes preferentially localize along actin-rich structures, supporting the link between MLP self-association and the actin cytoskeleton previously suggested by Boateng's biochemical analyses (22). Second, we found that the deletion of MLP C-terminal LIM domain (LIM2) is sufficient to abolish the interaction between MLP and AFs both in live cells and in reconstituted assays. This strongly suggests that LIM2 is the main actin-binding interface of MLP, which in turn implies that MLP has to self-associate in order to reach the bi-/multivalent conformation required to cross-link AFs. It is noteworthy, however, that a LIM2-only peptide (which includes the glycine-rich region following LIM2) (see Fig. S3 in the supplemental material) was unable to bind to AFs in high-speed cosedimentation assays, indicating that LIM2 is sufficient for an actin-binding domain. In further support of a link between MLP self-association and actin-bundling activity, our biochemical data indicate that under saturating conditions, MLP-induced bundles contained >1.5 molecule of MLP of per actin subunit.

The finding that the N-terminal LIM domain (LIM1) plays a critical role in MLP self-association suggests a model in which MLP self-associates via its N-terminal LIM domain and cross-links AFs via interacting C-terminal LIM (LIM2) domains. Interestingly, some of our data suggest that the actin cytoskeleton facilitates MLP self-association to some extent. First, and as previously stated, the highest BiFC signals are detected along actin stress fibers, whereas lower signals are detected in the cytosol and the nucleus. Second, the deletion of LIM2 (i.e., the domain that interacts with AFs) induces a moderate but statistically significant reduction of BiFC, indicating that fewer MLP complexes are formed when the protein is not bound to AFs. The fact that the deletion of LIM1 was sufficient to abrogate Venus complementa-

tion in BiFC assays indicates that LIM2 does not trigger MLP dimerization *per se*. Therefore, LIM2 likely acts as a facilitator of MLP self-association by locally increasing the concentration of MLP monomers along AF-rich structures.

In conclusion, the present study strongly supports the view that, in addition to its signaling functions, MLP plays a structural role through the cross-linking of AFs. So far, the mechanism(s) by which point mutations identified in human MLP contributes to heart disease remains unclear. In light of our data, it is highly conceivable that (some of) these mutations affect the ability of MLP to self-associate and/or to cross-link AFs. This hypothesis should be tested in future studies.

ACKNOWLEDGMENTS

This work was supported by the National Research Fund (FNR; C10/BM/784171-HUMCRP), the Fondation Cancer (FC/2013/03), and the Ministry of Culture, Higher Education and Research (REC-LBMV-20100902) of Luxembourg.

We are grateful to Tom Kerppola (University of Michigan Medical School) and Chang-Deng Hu (Purdue University, USA) for sharing BiFC plasmids, pFlag-Cerulean and pHA-Venus (A206K and I152L). We thank David Kovar (University of Chicago) and Simone Niclou (CRP-Santé, Luxembourg) for the gift of recombinant fascin and C2C12 cells, respectively. We also thank Petr Nazarov (CRP-Santé, Luxembourg) for his support in statistical analyses and Angela Tavares Furtado for technical assistance.

REFERENCES

1. **Arber S, Halder G, Caroni P.** 1994. Muscle LIM protein, a novel essential regulator of myogenesis, promotes myogenic differentiation. Cell **79:**221–231. http://dx.doi.org/10.1016/0092-8674(94)90192-9.
2. **Chang DF, Belaguli NS, Chang J, Schwartz RJ.** 2007. LIM-only protein, CRP2, switched on smooth muscle gene activity in adult cardiac myocytes. Proc. Natl. Acad. Sci. U. S. A. **104:**157–162. http://dx.doi.org/10.1073/pnas.0605635103.
3. **Chang DF, Belaguli NS, Iyer D, Roberts WB, Wu SP, Dong XR, Marx JG, Moore MS, Beckerle MC, Majesky MW, Schwartz RJ.** 2003. Cysteine-rich LIM-only proteins CRP1 and CRP2 are potent smooth muscle differentiation cofactors. Dev. Cell **4:**107–118. http://dx.doi.org/10.1016/S1534-5807(02)00396-9.
4. **Jarvinen PM, Myllarniemi M, Liu H, Moore HM, Lepparanta O, Salmenkivi K, Koli K, Latonen L, Band A, Laiho M.** 2012. Cysteine-rich protein 1 is regulated by transforming growth factor-beta1 and expressed in lung fibrosis. J. Cell. Physiol. **227:**2605–2612. http://dx.doi.org/10.1002/jcp.23000.
5. **Latonen L, Jarvinen PM, Laiho M.** 2008. Cytoskeleton-interacting LIM-domain protein CRP1 suppresses cell proliferation and protects from stress-induced cell death. Exp. Cell Res. **314:**738–747. http://dx.doi.org/10.1016/j.yexcr.2007.11.024.
6. **Wang X, Li Q, Adhikari N, Hall JL.** 2006. A role for muscle LIM protein (MLP) in vascular remodeling. J. Mol. Cell. Cardiol. **40:**503–509. http://dx.doi.org/10.1016/j.yjmcc.2006.01.005.
7. **Wei J, Gorman TE, Liu X, Ith B, Tseng A, Chen Z, Simon DI, Layne MD, Yet SF.** 2005. Increased neointima formation in cysteine-rich protein 2-deficient mice in response to vascular injury. Circ. Res. **97:**1323–1331. http://dx.doi.org/10.1161/01.RES.0000194331.76925.5c.
8. **Weiskirchen R, Bister K.** 1993. Suppression in transformed avian fibroblasts of a gene (crp) encoding a cysteine-rich protein containing LIM domains. Oncogene **8:**2317–2324.
9. **Weiskirchen R, Gunther K.** 2003. The CRP/MLP/TLP family of LIM domain proteins: acting by connecting. Bioessays **25:**152–162. http://dx.doi.org/10.1002/bies.10226.
10. **Kong Y, Flick MJ, Kudla AJ, Konieczny SF.** 1997. Muscle LIM protein promotes myogenesis by enhancing the activity of MyoD. Mol. Cell. Biol. **17:**4750–4760.
11. **Arber S, Caroni P.** 1996. Specificity of single LIM motifs in targeting and LIM/LIM interactions in situ. Genes Dev. **10:**289–300. http://dx.doi.org/10.1101/gad.10.3.289.
12. **Flick MJ, Konieczny SF.** 2000. The muscle regulatory and structural protein MLP is a cytoskeletal binding partner of betaI-spectrin. J. Cell Sci. **113**(Part 9)**:**1553–1564.
13. **Louis HA, Pino JD, Schmeichel KL, Pomies P, Beckerle MC.** 1997. Comparison of three members of the cysteine-rich protein family reveals functional conservation and divergent patterns of gene expression. J. Biol. Chem. **272:**27484–27491. http://dx.doi.org/10.1074/jbc.272.43.27484.
14. **Pomies P, Louis HA, Beckerle MC.** 1997. CRP1, a LIM domain protein implicated in muscle differentiation, interacts with alpha-actinin. J. Cell Biol. **139:**157–168. http://dx.doi.org/10.1083/jcb.139.1.157.
15. **Schmeichel KL, Beckerle MC.** 1998. LIM domains of cysteine-rich protein 1 (CRP1) are essential for its zyxin-binding function. Biochem. J. **331**(Part 3)**:**885–892.
16. **Geier C, Gehmlich K, Ehler E, Hassfeld S, Perrot A, Hayess K, Cardim N, Wenzel K, Erdmann B, Krackhardt F, Posch MG, Osterziel KJ, Bublak A, Nagele H, Scheffold T, Dietz R, Chien KR, Spuler S, Furst DO, Nurnberg P, Ozcelik C.** 2008. Beyond the sarcomere: CSRP3 mutations cause hypertrophic cardiomyopathy. Hum. Mol. Genet. **17:**2753–2765. http://dx.doi.org/10.1093/hmg/ddn160.
17. **Hershberger RE, Parks SB, Kushner JD, Li D, Ludwigsen S, Jakobs P, Nauman D, Burgess D, Partain J, Litt M.** 2008. Coding sequence mutations identified in MYH7, TNNT2, SCN5A, CSRP3, LBD3, and TCAP from 313 patients with familial or idiopathic dilated cardiomyopathy. Clin. Transl. Sci. **1:**21–26. http://dx.doi.org/10.1111/j.1752-8062.2008.00017.x.
18. **Knoll R, Hoshijima M, Hoffman HM, Person V, Lorenzen-Schmidt I, Bang ML, Hayashi T, Shiga N, Yasukawa H, Schaper W, McKenna W, Yokoyama M, Schork NJ, Omens JH, McCulloch AD, Kimura A, Gregorio CC, Poller W, Schaper J, Schultheiss HP, Chien KR.** 2002. The cardiac mechanical stretch sensor machinery involves a Z disc complex that is defective in a subset of human dilated cardiomyopathy. Cell **111:**943–955. http://dx.doi.org/10.1016/S0092-8674(02)01226-6.
19. **Mohapatra B, Jimenez S, Lin JH, Bowles KR, Coveler KJ, Marx JG, Chrisco MA, Murphy RT, Lurie PR, Schwartz RJ, Elliott PM, Vatta M, McKenna W, Towbin JA, Bowles NE.** 2003. Mutations in the muscle LIM protein and alpha-actinin-2 genes in dilated cardiomyopathy and endocardial fibroelastosis. Mol. Genet. Metab. **80:**207–215. http://dx.doi.org/10.1016/S1096-7192(03)00142-2.
20. **Newman B, Cescon D, Woo A, Rakowski H, Erikkson MJ, Sole M, Wigle ED, Siminovitch KA.** 2005. W4R variant in CSRP3 encoding muscle LIM protein in a patient with hypertrophic cardiomyopathy. Mol. Genet. Metab. **84:**374–375. http://dx.doi.org/10.1016/j.ymgme.2004.11.013.
21. **Bos JM, Poley RN, Ny M, Tester DJ, Xu X, Vatta M, Towbin JA, Gersh BJ, Ommen SR, Ackerman MJ.** 2006. Genotype-phenotype relationships involving hypertrophic cardiomyopathy-associated mutations in titin, muscle LIM protein, and telethonin. Mol. Genet. Metab. **88:**78–85. http://dx.doi.org/10.1016/j.ymgme.2005.10.008.
22. **Boateng SY, Belin RJ, Geenen DL, Margulies KB, Martin JL, Hoshijima M, de Tombe PP, Russell B.** 2007. Cardiac dysfunction and heart failure are associated with abnormalities in the subcellular distribution and amounts of oligomeric muscle LIM protein. Am. J. Physiol. Heart Circ. Physiol. **292:**H259–H269. http://dx.doi.org/10.1152/ajpheart.00766.2006.
23. **Zolk O, Caroni P, Bohm M.** 2000. Decreased expression of the cardiac LIM domain protein MLP in chronic human heart failure. Circulation **101:**2674–2677. http://dx.doi.org/10.1161/01.CIR.101.23.2674.
24. **Arber S, Hunter JJ, Ross J, Jr, Hongo M, Sansig G, Borg J, Perriard JC, Chien KR, Caroni P.** 1997. MLP-deficient mice exhibit a disruption of cardiac cytoarchitectural organization, dilated cardiomyopathy, and heart failure. Cell **88:**393–403. http://dx.doi.org/10.1016/S0092-8674(00)81878-4.
25. **Knoll R, Kostin S, Klede S, Savvatis K, Klinge L, Stehle I, Gunkel S, Kotter S, Babicz K, Sohns M, Miocic S, Didie M, Knoll G, Zimmermann WH, Thelen P, Bickeboller H, Maier L, Schaper W, Schaper J, Kraft T, Tschope C, Linke WA, Chien KR.** 2010. A common MLP (muscle LIM protein) variant is associated with cardiomyopathy. Circ. Res. **106:**695–704. http://dx.doi.org/10.1161/CIRCRESAHA.109.206243.
26. **Buyandelger B, Ng KE, Miocic S, Piotrowska I, Gunkel S, Ku CH, Knoll R.** 2011. MLP (muscle LIM protein) as a stress sensor in the heart. Pflugers Arch. **462:**135–142. http://dx.doi.org/10.1007/s00424-011-0961-2.
27. **Heineke J, Ruetten H, Willenbockel C, Gross SC, Naguib M, Schaefer A, Kempf T, Hilfiker-Kleiner D, Caroni P, Kraft T, Kaiser RA, Molkentin JD, Drexler H, Wollert KC.** 2005. Attenuation of cardiac remodeling after myocardial infarction by muscle LIM protein-calcineurin sig-

naling at the sarcomeric Z-disc. Proc. Natl. Acad. Sci. U. S. A. **102:**1655–1660. http://dx.doi.org/10.1073/pnas.0405488102.
28. **Boateng SY, Senyo SE, Qi L, Goldspink PH, Russell B.** 2009. Myocyte remodeling in response to hypertrophic stimuli requires nucleocytoplasmic shuttling of muscle LIM protein. J. Mol. Cell. Cardiol. **47:**426–435. http://dx.doi.org/10.1016/j.yjmcc.2009.04.006.
29. **Ecarnot-Laubriet A, De Luca K, Vandroux D, Moisant M, Bernard C, Assem M, Rochette L, Teyssier JR.** 2000. Downregulation and nuclear relocation of MLP during the progression of right ventricular hypertrophy induced by chronic pressure overload. J. Mol. Cell. Cardiol. **32:**2385–2395. http://dx.doi.org/10.1006/jmcc.2000.1269.
30. **Grubinger M, Gimona M.** 2004. CRP2 is an autonomous actin-binding protein. FEBS Lett. **557:**88–92. http://dx.doi.org/10.1016/S0014-5793(03)01451-0.
31. **Kihara T, Shinohara S, Fujikawa R, Sugimoto Y, Murata M, Miyake J.** 2011. Regulation of cysteine-rich protein 2 localization by the development of actin fibers during smooth muscle cell differentiation. Biochem. Biophys. Res. Commun. **411:**96–101. http://dx.doi.org/10.1016/j.bbrc.2011.06.100.
32. **Tran TC, Singleton C, Fraley TS, Greenwood JA.** 2005. Cysteine-rich protein 1 (CRP1) regulates actin filament bundling. BMC Cell Biol. **6:**45. http://dx.doi.org/10.1186/1471-2121-6-45.
33. **Jang HS, Greenwood JA.** 2009. Glycine-rich region regulates cysteine-rich protein 1 binding to actin cytoskeleton. Biochem. Biophys. Res. Commun. **380:**484–488. http://dx.doi.org/10.1016/j.bbrc.2009.01.125.
34. **Ma L, Greenwood JA, Schachner M.** 2011. CRP1, a protein localized in filopodia of growth cones, is involved in dendritic growth. J. Neurosci. **31:**16781–16791. http://dx.doi.org/10.1523/JNEUROSCI.2595-11.2011.
35. **Clark KA, Kadrmas JL.** 2013. Drosophila melanogaster muscle LIM protein and alpha-actinin function together to stabilize muscle cytoarchitecture: a potential role for Mlp84B in actin-crosslinking. Cytoskeleton (Hoboken) **70:**304–316. http://dx.doi.org/10.1002/cm.21106.
36. **Higaki T, Kutsuna N, Sano T, Kondo N, Hasezawa S.** 2010. Quantification and cluster analysis of actin cytoskeletal structures in plant cells: role of actin bundling in stomatal movement during diurnal cycles in Arabidopsis guard cells. Plant J. **61:**156–165. http://dx.doi.org/10.1111/j.1365-313X.2009.04032.x.
37. **Papuga J, Hoffmann C, Dieterle M, Moes D, Moreau F, Tholl S, Steinmetz A, Thomas C.** 2010. Arabidopsis LIM proteins: a family of actin bundlers with distinct expression patterns and modes of regulation. Plant Cell **22:**3034–3052. http://dx.doi.org/10.1105/tpc.110.075960.
38. **Hoffmann C, Moes D, Dieterle M, Neumann K, Moreau F, Tavares Furtado A, Dumas D, Steinmetz A, Thomas C.** 2014. Live cell imaging approaches reveal actin cytoskeleton-induced self-association of the actin-bundling protein WLIM1. J. Cell Sci. **127**(Part 3)**:**583–598. http://dx.doi.org/10.1242/jcs.134536.
39. **Claycomb WC, Lanson NA, Jr, Stallworth BS, Egeland DB, Delcarpio JB, Bahinski A, Izzo NJ, Jr.** 1998. HL-1 cells: a cardiac muscle cell line that contracts and retains phenotypic characteristics of the adult cardiomyocyte. Proc. Natl. Acad. Sci. U. S. A. **95:**2979–2984. http://dx.doi.org/10.1073/pnas.95.6.2979.
40. **Skau CT, Courson DS, Bestul AJ, Winkelman JD, Rock RS, Sirotkin V, Kovar DR.** 2011. Actin filament bundling by fimbrin is important for endocytosis, cytokinesis, and polarization in fission yeast. J. Biol. Chem. **286:**26964–26977. http://dx.doi.org/10.1074/jbc.M111.239004.
41. **Royston P.** 1982. Algorithm AS 181: the W test for normality. Appl. Stat. **31:**176–180. http://dx.doi.org/10.2307/2347986.
42. **Harris ES, Rouiller I, Hanein D, Higgs HN.** 2006. Mechanistic differences in actin bundling activity of two mammalian formins, FRL1 and mDia2. J. Biol. Chem. **281:**14383–14392. http://dx.doi.org/10.1074/jbc.M510923200.
43. **Breitsprecher D, Kiesewetter AK, Linkner J, Faix J.** 2009. Analysis of actin assembly by in vitro TIRF microscopy. Methods Mol. Biol. **571:**401–415. http://dx.doi.org/10.1007/978-1-60761-198-1_27.
44. **Papalouka V, Arvanitis DA, Vafiadaki E, Mavroidis M, Papadodima SA, Spiliopoulou CA, Kremastinos DT, Kranias EG, Sanoudou D.** 2009. Muscle LIM protein interacts with cofilin 2 and regulates F-actin dynamics in cardiac and skeletal muscle. Mol. Cell. Biol. **29:**6046–6058. http://dx.doi.org/10.1128/MCB.00654-09.
45. **Sheahan MB, Staiger CJ, Rose RJ, McCurdy DW.** 2004. A green fluorescent protein fusion to actin-binding domain 2 of Arabidopsis fimbrin highlights new features of a dynamic actin cytoskeleton in live plant cells. Plant Physiol. **136:**3968–3978. http://dx.doi.org/10.1104/pp.104.049411.
46. **White SM, Constantin PE, Claycomb WC.** 2004. Cardiac physiology at the cellular level: use of cultured HL-1 cardiomyocytes for studies of cardiac muscle cell structure and function. Am. J. Physiol. Heart Circ. Physiol. **286:**H823–H829. http://dx.doi.org/10.1152/ajpheart.00986.2003.
47. **Mery A, Taghli-Lamallem O, Clark KA, Beckerle MC, Wu X, Ocorr K, Bodmer R.** 2008. The Drosophila muscle LIM protein, Mlp84B, is essential for cardiac function. J. Exp. Biol. **211:**15–23. http://dx.doi.org/10.1242/jeb.012435.
48. **Khurana P, Henty JL, Huang S, Staiger AM, Blanchoin L, Staiger CJ.** 2010. Arabidopsis VILLIN1 and VILLIN3 have overlapping and distinct activities in actin bundle formation and turnover. Plant Cell **22:**2727–2748. http://dx.doi.org/10.1105/tpc.110.076240.
49. **Michelot A, Derivery E, Paterski-Boujemaa R, Guerin C, Huang S, Parcy F, Staiger CJ, Blanchoin L.** 2006. A novel mechanism for the formation of actin-filament bundles by a nonprocessive formin. Curr. Biol. **16:**1924–1930. http://dx.doi.org/10.1016/j.cub.2006.07.054.
50. **Hu CD, Chinenov Y, Kerppola TK.** 2002. Visualization of interactions among bZIP and Rel family proteins in living cells using bimolecular fluorescence complementation. Mol. Cell **9:**789–798. http://dx.doi.org/10.1016/S1097-2765(02)00496-3.
51. **Rizzo MA, Springer GH, Granada B, Piston DW.** 2004. An improved cyan fluorescent protein variant useful for FRET. Nat. Biotechnol. **22:**445–449. http://dx.doi.org/10.1038/nbt945.
52. **Kodama Y, Hu CD.** 2010. An improved bimolecular fluorescence complementation assay with a high signal-to-noise ratio. Biotechniques **49:**793–805. http://dx.doi.org/10.2144/000113519.
53. **Kadrmas JL, Beckerle MC.** 2004. The LIM domain: from the cytoskeleton to the nucleus. Nat. Rev. Mol. Cell. Biol. **5:**920–931. http://dx.doi.org/10.1038/nrm1499.
54. **Gupta MP, Samant SA, Smith SH, Shroff SG.** 2008. HDAC4 and PCAF bind to cardiac sarcomeres and play a role in regulating myofilament contractile activity. J. Biol. Chem. **283:**10135–10146. http://dx.doi.org/10.1074/jbc.M710277200.
55. **Ehler E, Horowits R, Zuppinger C, Price RL, Perriard E, Leu M, Caroni P, Sussman M, Eppenberger HM, Perriard JC.** 2001. Alterations at the intercalated disk associated with the absence of muscle LIM protein. J. Cell Biol. **153:**763–772. http://dx.doi.org/10.1083/jcb.153.4.763.
56. **Djinovic-Carugo K, Young P, Gautel M, Saraste M.** 1999. Structure of the alpha-actinin rod: molecular basis for cross-linking of actin filaments. Cell **98:**537–546. http://dx.doi.org/10.1016/S0092-8674(00)81981-9.
57. **Gehmlich K, Geier C, Osterziel KJ, Van der Ven PF, Furst DO.** 2004. Decreased interactions of mutant muscle LIM protein (MLP) with N-RAP and alpha-actinin and their implication for hypertrophic cardiomyopathy. Cell Tissue Res. **317:**129–136. http://dx.doi.org/10.1007/s00441-004-0873-y.
58. **Sjoblom B, Salmazo A, Djinovic-Carugo K.** 2008. Alpha-actinin structure and regulation. Cell. Mol. Life Sci. **65:**2688–2701. http://dx.doi.org/10.1007/s00018-008-8080-8.
59. **Breitsprecher D, Koestler SA, Chizhov I, Nemethova M, Mueller J, Goode BL, Small JV, Rottner K, Faix J.** 2011. Cofilin cooperates with fascin to disassemble filopodial actin filaments. J. Cell Sci. **124:**3305–3318. http://dx.doi.org/10.1242/jcs.086934.
60. **Courson DS, Rock RS.** 2010. Actin cross-link assembly and disassembly mechanics for alpha-actinin and fascin. J. Biol. Chem. **285:**26350–26357. http://dx.doi.org/10.1074/jbc.M110.123117.
61. **Ishikawa R, Sakamoto T, Ando T, Higashi-Fujime S, Kohama K.** 2003. Polarized actin bundles formed by human fascin-1: their sliding and disassembly on myosin II and myosin V in vitro. J. Neurochem. **87:**676–685. http://dx.doi.org/10.1046/j.1471-4159.2003.02058.x.
62. **Liu J, Taylor DW, Taylor KA.** 2004. A 3-D reconstruction of smooth muscle alpha-actinin by CryoEm reveals two different conformations at the actin-binding region. J. Mol. Biol. **338:**115–125. http://dx.doi.org/10.1016/j.jmb.2004.02.034.
63. **Hampton CM, Taylor DW, Taylor KA.** 2007. Novel structures for alpha-actinin:F-actin interactions and their implications for actin-membrane attachment and tension sensing in the cytoskeleton. J. Mol. Biol. **368:**92–104. http://dx.doi.org/10.1016/j.jmb.2007.01.071.